31 August 1973, Volume 181, Number 4102 SCIENCE

Earthquake Prediction: A Physical Basis

Rock dilatancy and water diffusion may explain a large class of phenomena precursory to earthquakes.

Christopher H. Scholz, Lynn R. Sykes, Yash P. Aggarwal

Earthquake prediction, an old and elusive goal of seismologists and astrologers alike, appears to be on the verge of practical reality as a result of recent advances in the earth and materials sciences.

A variety of effects premonitory to earthquakes such as crustal movements and anomalous changes in such phenomena as tilt, fluid pressure, electrical and magnetic fields, radon emission, the frequency of occurrence of small local earthquakes, and the ratio of the number of small to large shocks have been observed before various earthquakes. Until a few years ago many earth scientists were dubious about the validity of these observations and were even more uncertain about whether these effects were characteristic of more than a few earthquakes. Vigorous programs to monitor premonitory effects, particularly those in Japan and the U.S.S.R. during the last 5 to 10 years, leave little doubt that such effects are real.

In 1969 seismologists in the U.S.S.R. found premonitory changes in the ratio of the seismic compressional velocity to the seismic shear velocity (v_P/v_S) prior to a series of earthquakes of moderate size in the Garm region of central Asia (*1*). Nearly identical results were reported recently for somewhat smaller earthquakes in the Adirondack region of New York State (*2*). The discovery of a similar anomaly in velocity that occurred 3½ years before the disastrous San Fernando, California, earthquake of February 1971 (*3*) leaves little doubt of the potential applicability of precursory effects to the prediction of at least certain classes of large and destructive earthquakes.

Our aim in this article is to show that precursory effects occur before many, and perhaps all, shallow earthquakes and to demonstrate that heretofore unrelated premonitory phenomena have a common physical basis. These premonitory effects occur at a characteristic time before earthquakes that increases with the earthquake's magnitude and that appears to be related to the time needed for the formation of cracks and for the diffusion of fluids through the volume of rock in the earthquake source region. It is important to note that every one of the premonitory effects found in field observations has been reported in rock mechanics studies in the laboratory. Thus, a program of observation, data reduction, and research appears to us to have good prospects as a method for predicting the time, place, and size of many earthquakes. Fortunately, the mechanism of premonitory changes appears to lead to prediction which is deterministic rather than probabilistic.

The Dilatancy Model

Observations for a number of earthquakes made at Garm, U.S.S.R., and in the New York Adirondacks and observations of the San Fernando earthquake show that, prior to each of these earthquakes, the ratio of seismic velocities v_P/v_S decreased to anomalously low values. In each of these cases, earthquakes occurred shortly after the return of v_P/v_S to its normal value.

Nur (*4*) and Aggarwal *et al.* (*2*) independently put forward a model that would explain this phenomenon. The model is based on laboratory fracture studies which show that rock undergoes an inelastic volumetric increase prior to failure, a phenomenon known as dilatancy (*5*). Dilatancy is produced by the formation and propagation of cracks within the rock, and begins to occur at stresses as low as half the breaking strength. Laboratory data also indicate that the observed v_P/v_S anomalies can be explained on the assumption that dilatancy precedes the earthquake (*6*). This model is attractive because the very low values of v_P/v_S observed prior to the earthquakes (which indicate a Poisson's ratio of about 0.1) would be very difficult to explain in any other way.

The low v_P/v_S ratio occurs because dilatancy causes the rock to become undersaturated, which will strongly reduce v_P but will have little effect on v_S. The sequence of events is shown in Fig. 1, which gives laboratory data on the dependence of v_P and v_S on effective pressure (total pressure minus pore pressure) for saturated and dry rock. The process can be divided into three stages. Stage I consists of the accumulation of tectonic strain, which produces a slow, steady increase of effective stress. At point *b*, the stress has become large enough to begin producing dilatancy at a rate faster

Dr. Scholz is a senior research associate at the Lamont-Doherty Geological Observatory of Columbia University, Palisades, New York 10964. Dr. Sykes is professor of geology at Columbia University and head of the seismology group at Lamont-Doherty Geological Observatory. Mr. Aggarwal is a graduate student at the Observatory.

than the rate at which pore water can flow into the newly created pore volume. The rock becomes undersaturated, and v_P begins to drop, following the path *bc* (stage II). Since v_S is scarcely affected by the presence of water, v_P/v_S also decreases.

Along *bc*, the pore pressure in the dilatant region will drop as water flows from nearby cracks and pores into the newly formed cracks, and thus the effective stress will rise. This will result in a strengthening of the rock (dilatancy hardening) (*7*) which will progressively inhibit further dilatancy until a point is reached (point *c*) at which the rate of fluid flow into the dilatant region from surrounding areas dominates dilatancy and the rock begins to become more saturated. At this point stage III begins, and v_P increases along *cd*. The pore pressure may still be dropping at this time. This is so because undersaturation does not imply that the pore pressure is zero, since some time will be required to allow the water to flow into the newly formed cracks from the adjacent cracks and pores. Hence the minimum in pore pressure will occur at point *d*, where the rock is saturated again.

At point *d*, v_P/v_S has resumed its normal value and the pore pressure begins to increase to the ambient level along the path *de*. Since the tectonic stress has continued to rise during the dilatant period, the rising pore pressure along *de* triggers the earthquake, just as it does through fluid injection or reservoir filling (*8*). A comparison of laboratory friction and fracture data (*9*) indicates that the stress necessary to cause frictional sliding on a favorably oriented fault is just inside the dilatant region of the equivalent unfractured rock. Dilatancy thus delays the earthquake by reducing the fluid pressure on the fault and then triggers it when the pore pressure is recovered. The time delay between the two events depends on the rate at which the dilatancy develops and the rate at which water can flow into the dilatant zone. The latter depends upon the size of the dilatant zone; hence the duration of the dilatancy anomaly will be a function of the size of the earthquake that follows it.

The model given in Fig. 1 is simplified in the sense that it implies that all points in the dilatant volume are at the same stage simultaneously. The actual situation in three dimensions involves the diffusion of water as well as possible spatial variations in dilatancy rates, which may tend to smear out the behavior somewhat in space and time.

Blue Mountain Lake Data

Aggarwal *et al.* (*2*) have reported changes in the velocity ratio (Fig. 2, B and C) premonitory to two events of moderate size and a number of smaller events in the Blue Mountain Lake (BML), New York, earthquake swarm of 1971. Figure 2A shows a similar but particularly clear anomaly in v_P/v_S prior to another BML earthquake in the same series. Arrows indicate the times of occurrence and the relative sizes of all shocks larger than magnitude $(M) = 1$. In all three cases, the velocity ratio at first decreased and subsequently increased gradually to its normal value prior to the largest shock. The earthquake, however, occurred some time after v_P/v_S attained its normal value. The delay between the end of the v_P/v_S anomaly and the occurrence time of the earthquake was 15 to 25 percent of the time duration of the anomaly, where this time duration is taken as the total time from the moment v_P/v_S started decreasing to the occurrence of the earthquake. During periods in which no earthquake larger than $M = 1$ occurred (Fig. 2D and after the largest shocks in Fig. 2, A to C) the velocity ratio remained relatively constant, fluctuating around a mean value of about 1.75. The time duration of the anomaly prior to the 20 June event ($M = 3.1$) (Fig. 2A) is slightly less than that for the 10 July event ($M = 3.3$) (Fig. 2B) and appreciably longer than for the 27 July event ($M = 2.5$) (Fig. 2C). The magnitude of the decrease in v_P/v_S does not, however, show any apparent dependence on the size of the earthquake.

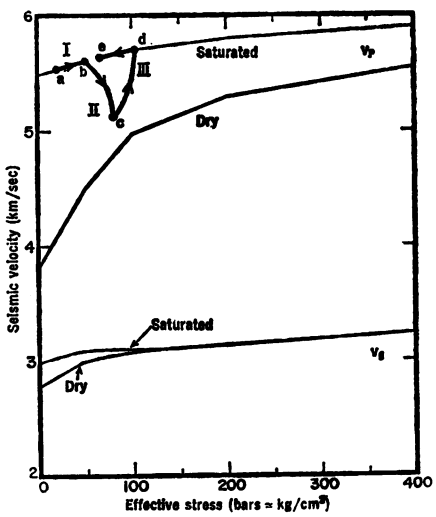

Fig. 1. Seismic velocities v_P and v_S as a function of the effective confining pressure for wet and dry Westerly granite (*6*). The P wave velocity follows along the direction of the arrows as dilatancy occurs in the earthquake source region (see text). The S wave velocity is scarcely affected, and arrows are therefore omitted. Roman numerals indicate stages in the earthquake cycle. Our diagram is similar to that of Whitcomb and Garmany (*3*) except for the addition of the path *de*.

A detailed study of the changes of P wave velocity in and around the focal zone of the BML earthquakes, based on the arrival times of P waves from nearby quarry blasts, is in progress. Preliminary data indicate that the decrease in the velocity ratio prior to the three BML events was attributable primarily to a decrease in the P velocity of about 15 percent. Whitcomb and Garmany (*3*) reached a similar conclusion for the 1971 San Fernando earthquake.

The pattern of the anomalous changes in v_P/v_S prior to the BML earthquakes is in complete agreement with that predicted from the dilatancy model. The various stages of the earthquake cycle are shown in Fig. 2A. In addition, the dilatancy model predicts that, as pore pressure decreases and effective stress increases during stage II and part of stage III (Fig. 1), dilatancy hardening should occur and the seismic activity should decrease. Figure 2E shows, on the same time scale as Fig. 2C, the number of microearthquakes for 3-hour periods before and after the 27 July event. Several short periods of poor record quality are indicated by zero counts. A clear indication of a slight drop in seismic activity as v_P/v_S decreased (Fig. 2C) is evident in Fig. 2E. The seismic activity, however, did not increase as v_P/v_S subsequently increased, but decreased further, reaching a pronounced minimum around 25 to 26 July. We pointed out earlier that during the initial part of stage III (path *cd*, Fig. 1), although the degree of saturation increases in the dilatant zone and v_P/v_S increases, the pore pressure may continue to decrease, and hence dilatancy hardening may persist until point *d* (Fig. 1) is reached and v_P/v_S has nearly attained its normal value. Along *de* (Fig. 1) the pore pressure increases and the model predicts an increase in seismicity. Such a subsequent general increase in the number of microearthquakes is clearly seen

in Fig. 2E. Sadovsky *et al.* (*10*) report a similar decrease and subsequent increase in seismic activity prior to an $M = 6$ shock near Garm, U.S.S.R.

Other Precursory Effects

The dilatancy responsible for the v_P/v_S anomaly observed to precede earthquakes will by its nature manifest itself in other changes in the source region, many of which may be readily observable. In recent years much effort has been devoted to finding precursors to earthquakes, and many diverse phenomena have been observed. In studying these precursors, it becomes obvious that they fall into two main classes: short-term effects, which precede the earthquake by a few hours to days, even for very large events, and long-term precursors, which precede large earthquakes by months to years. An examination of the long-term precursors shows that most, if not all, of this class of precursors can be attributed to the same dilatancy mechanism as was introduced to explain the v_P/v_S anomaly.

On the basis of laboratory studies of dilatancy and its effects, various other types of precursory phenomena are implied by the dilatancy model. In Fig. 3 we schematically show the behavior of various phenomena predicted by the model. At the top of Fig. 3 is shown the variation in the v_P/v_S anomaly, discussed earlier. Another precursor directly implied by dilatancy is crustal uplift in the epicentral region which may be detected by geodetic or tilt measurements. The amount of strain required to produce the observed v_P/v_S anomaly can be estimated from laboratory data (*5*) to be of the order of 10^{-6} to 10^{-5}. If the dilatant zone is large and shallow enough, this amount of dilatancy would produce a crustal uplift of several centimeters, easily detectable with tiltmeters or precise leveling. The sequence of crustal movements predicted by the dilatancy model is shown schematically in Fig. 3. After a long period of tectonic strain accumulation, a more rapid crustal uplift of several centimeters will occur

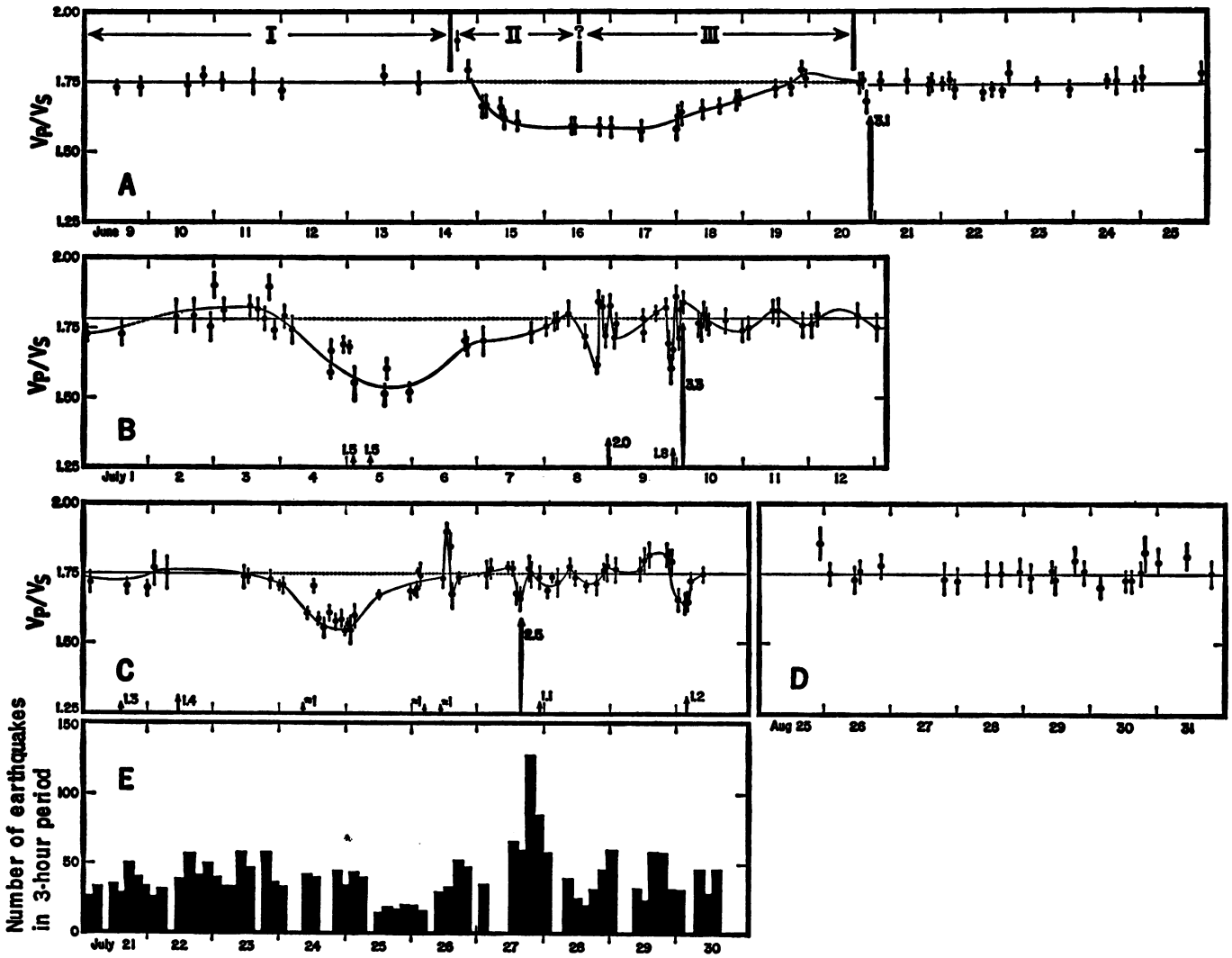

Fig. 2. (A–C) The velocity ratio v_P/v_S as a function of time before and after three of the largest events in the Blue Mountain Lake, New York, earthquake swarm of 1971. Vertical bars indicate standard deviations in the v_P/v_S measurement; arrows and numbers indicate, respectively, times of occurrence and the magnitudes of all earthquakes larger than $M = 1$. Stages in the earthquake cycle are indicated with Roman numerals in (A). (D) A similar plot of v_P/v_S for a period of time during which no earthquake larger than $M = 1$ occurred. Note the absence of anomalous changes in v_P/v_S. (E) The number of microearthquakes during successive 3-hour periods for several days before and after the $M = 2.5$ event on 27 July. Several short periods of poor record quality are indicated by zero counts. Note the drop in seismic activity as v_P/v_S decreases and the continued decrease even as v_P/v_S subsequently increases. Only after v_P/v_S nearly reaches its normal value does the seismic activity increase, as predicted by the dilatancy model.

during dilatancy, in stage II. Stage III, during which the dilatancy rate is slow or terminated and pore water is flowing into the dilated region, will be accompanied by little vertical crustal movement. We also include in Fig. 3 a stage IV to represent a possible stage of very rapid movement just prior to the earthquake as is suggested by short-term precursory phenomena but which is not per se predicted by the dilatancy model. This stage may mark the beginning of stable sliding on the fault (*11*). Stage V is the earthquake itself, and stage VI is the period of readjustment during the aftershock sequence.

The presence of cracks and pore fluids, and hence dilatancy, affects many of the physical properties of rock. Among the properties most strongly affected is electrical resistivity (*5*). The electrical resistivity of rock depends mainly on the amount of water it contains, and laboratory fracture experiments with saturated rocks show

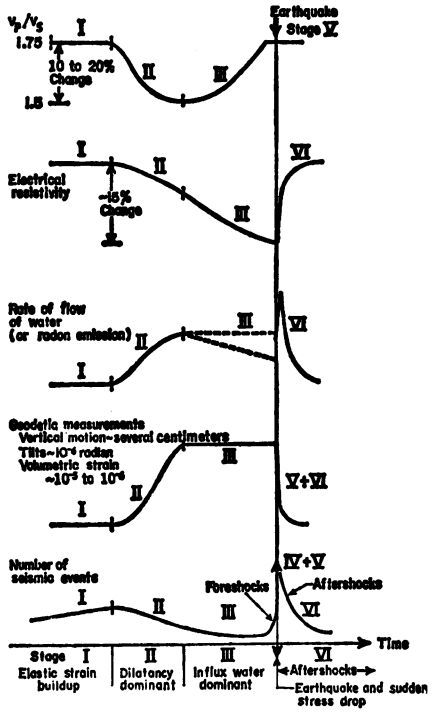

Fig. 3. Predicted changes in various physical parameters as a function of time during the earthquake cycle for the dilatancy model. Roman numerals indicate various stages in the cycle. Short-term fluctuations (stage IV), which are observed before some large earthquakes, are not indicated on the sketches. Note the striking correspondence between predicted premonitory effects and those observed (Figs. 4 to 7). The rate of water flow in stage III may vary as indicated by the dotted lines (see text). Radon emission may be a function not only of the rate of water flow but also of the rate of creation of new surface area by the growth of cracks.

that a marked decrease in resistivity occurs during dilatancy. Since dilatancy will be accompanied by an influx of water into the dilatant zone from its surroundings, a decrease in the electrical resistivity of the dilatant zone is expected to begin in stage II and continue through stage III (Fig. 3). Unlike the case for the v_P/v_S anomaly, resistivity will not return to its normal value but will continue to decrease until the earthquake occurs. The stress reduction produced by the earthquake will allow cracks to close and will force water from the source region, and the resistivity will rise toward its earlier value during stage VI.

Another precursory phenomenon is that the rate of flow of water in the rocks of the dilatant zone and its surroundings will be increased severalfold. Sensitive measures of flow rates, such as emission counts of short-lived isotopes like radon, will thus be influenced by dilatancy (Fig. 3). Seismicity will also be influenced, as there is a drop in activity due to dilatancy hardening in stage II and a rise again after point *d* in stage III (Fig. 1), that is, after the end of the v_P/v_S anomaly. This effect produces a period of anomalous quiescence for some time before the earthquake and a relatively short period of enhanced activity just prior to the main shock. This is the pattern of foreshocks observed before many larger earthquakes, and dilatancy hardening may generally explain why this pattern prevails instead of a gradual increase in seismicity leading up to the main shock, as might otherwise be expected (*5*). The *b* value, that is, the slope of the earthquake frequency-magnitude relation, will also be affected. Laboratory fracture studies and theoretical considerations indicate that the *b* value should decrease with increasing effective differential stress (*12*). We would therefore expect a decrease in the *b* value for most of stages II and III, where dilatancy hardening occurs, since the local stress required to cause fracturing during that period of time must be greater than prior to the hardening. Here again, the *b* value should increase just before the earthquake.

The most commonly reported long-term precursory phenomena are anomalous crustal movements. A particularly well-documented case is the 1964 ($M = 7.5$) Niigata earthquake. Repeated geodetic measurements in the epicentral region (Fig. 4) indicate that vertical movements had been occurring at a slow steady rate from 1898 to 1955, but, beginning in 1958, a rapid uplift of nearly 5 centimeters occurred in the epicentral region (*13*). This was followed by a 5-year period of little movement, terminated by the earthquake. The absolute nature of the uplift was confirmed by a corresponding drop in the mean sea level at the nearby tide station at Nezugaseki (Fig. 4). The magnitude of the precursory uplift decreased gradually with distance in both directions from the epicenter and was not observed at distances greater than about 100 kilometers. This spatial and temporal pattern is exactly what is expected from the dilatancy model. Thus, for this earthquake, the period from 1898 to 1958 is interpreted as stage I, a slow period of tectonic strain accumulation. Indeed, the movements produced by the earthquake itself were generally the reverse of these movements, as would be expected from elastic rebound. The period of rapid uplift, 1958 to 1959, is interpreted as dilatancy in stage II, and 1959 to 1964

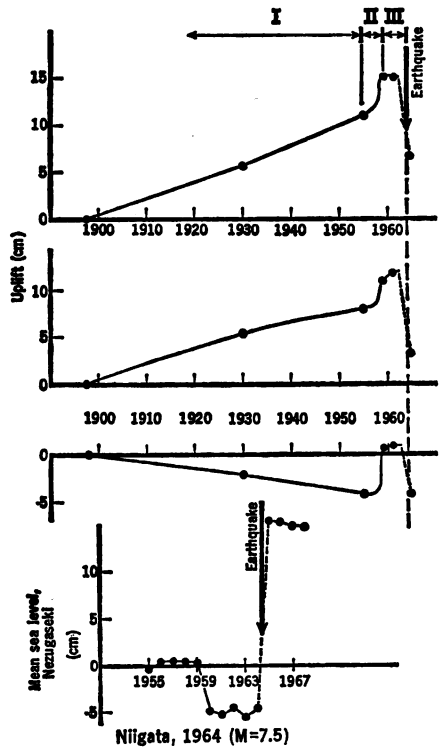

Fig. 4. The top three curves are elevation differences for three selected bench marks along a leveling route resurveyed several times before the 1964 earthquake at Niigata, Japan. The bottom curve presents mean sea level data from a tide gauge at Nezugaseki, near Niigata (a drop in sea level indicates uplift of the land). The recognizable stages in the earthquake cycle are indicated by Roman numerals. Note that premonitory effects are evident 6 years before this earthquake, $M = 7.5$. Data from (*13*).

is interpreted as stage III, where dilatancy has decreased and pore fluids are flowing into the dilated region, producing little crustal movement. This interpretation is strengthened by the observations that the rapid uplift is localized in the near epicentral region and that the maximum magnitude of the anomaly (5 centimeters) is about right for the dilatational strain (10^{-6} to 10^{-5}) expected over a source several tens of kilometers in dimensions. The dilatant region extended over a distance of 100 kilometers, which is about twice the fault length of this earthquake. Anomalous rates of change of the magnetic field were also observed in the vicinity of Niigata for about 10 years prior to the earthquake (*14*). It is likely that a redistribution of pore water affected by dilatancy could produce such a change in the magnetic field through its strong influence on electrical resistivity, or through the piezomagnetic effect produced by the increase in effective stress.

Tiltmeters have recorded several cases of precursory crustal movements. In one such example, an $M = 6$ earthquake at Odaigahara, Japan, in 1960, five tiltmeters at different localities up to 100 kilometers from the epicenter detected precursory movements (*15*). Six months prior to the earthquake, rapid tilting in the direction away from the epicenter began to be recorded at two locations, 40 and 100 kilometers, respectively, from the epicenter. A strainmeter at one of the sites began to show anomalously high rates of extension simultaneously. This continued for 3 months and then stopped, at which time a station farther to the south began tilting. One month before the earthquake, these three stations began tilting in the opposite direction and two additional stations began to tilt rapidly. These data also show distinctive stages II and III, although these stages occurred at different times in different localities, and both the magnitude and the duration of the tilts are explicable on the basis of the dilatancy model. The reversal of tilt just prior to the earthquake indicates some type of short-term precursor, perhaps due to a slight compaction of the dilatant volume.

Anomalous tilting preceded the Danville, California ($M = 4.5$), earthquake of 1971 by 1 month (*16*). In this case also there was a short-term precursory tilt toward the epicenter for 10 hours before the earthquake. These tilt observations are more complex than those obtained by leveling. The precursory

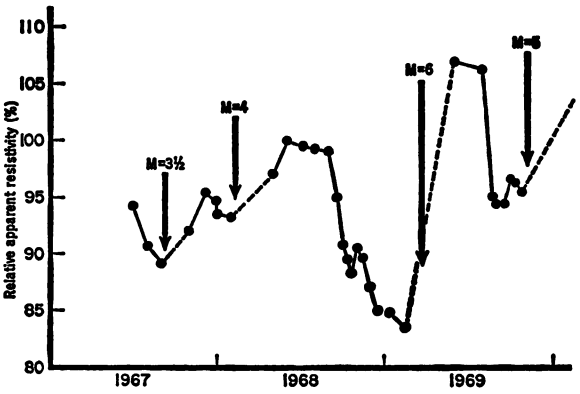

Fig. 5. Electrical resistivity anomalies observed before earthquakes at Garm, U.S.S.R. Note the marked drop in resistivity in the half-year period before the earthquake of $M = 6$ and the subsequent increase during and after the earthquake (*10*).

tilts are not often radially away from the epicenter. This finding may mean that the dilatant volume does not have simple spherical geometry, or, as is likely, it may mean that the tiltmeters are recording local perturbations of the strain field due to the inhomogeneity of the crust.

We have pointed out above that, according to the dilatancy model, there would be a significant reduction of the electrical resistivity prior to an earthquake as a result of the influx of water into the dilatant region. Long-baseline (6 kilometers) resistivity measurements have been made in the Garm region of the U.S.S.R. since 1967 (*10*). These data are given in Fig. 5, together with the occurrence times of all earthquakes of $M > 3$ which occurred within 10 kilometers of the baseline. A strong correlation exists between minima in electrical resistivity and the occurrence of earthquakes, as would be predicted by the model. Laboratory studies of the electrical resistivity of rocks show that it would be very difficult to explain these drops in resistivity in any other way except as an increase in the pore water content of the rocks (*5, 10*).

An even more striking phenomenon, almost undoubtedly the result of dilatancy, was observed to precede the 1966 Tashkent earthquake. Analysis of waters from a deep well in the hypocentral region showed an interesting variation in the radon content prior (*17*) to the earthquake (Fig. 6A). Several years prior to the earthquake the radon content increased very rapidly, doubling its normal value. The radon content was maintained at this high value until the earthquake, at which time, or soon after, it returned to its normal value. The same pattern was repeated prior to the larger aftershocks, on a shorter time scale (Fig. 6B).

Radon has a half-life of only 3.8 days, and its lifetime diffusion distance is only several centimeters. Thus its increased concentration in the Tashkent well prior to the earthquake and its larger aftershocks could have been caused by only two means: either by an increase in the surface area of rock in the epicentral region due to cracking, or by an increase in the flow rate of pore water. Both of these effects are predicted by the dilatancy model. In this case also (Fig. 6), the distinctive stages are again recognizable. It is significant that a very low v_P of 4.5 kilometers per second and a v_P/v_S

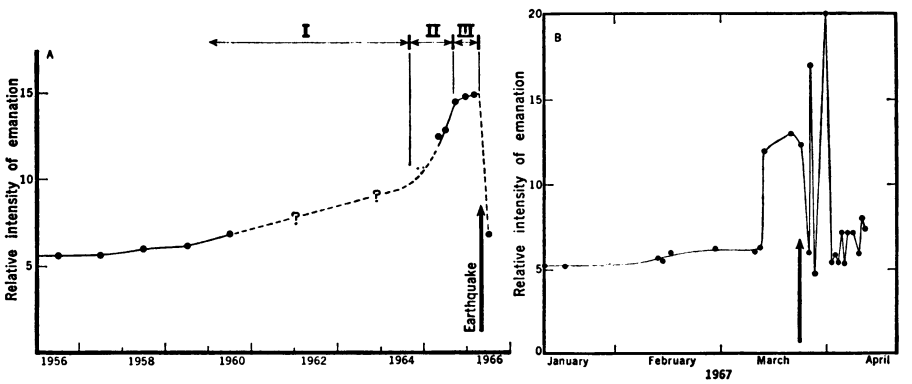

Fig. 6. Radon emission counts (*17*) from a deep well in the hypocentral zone of (A) the 1966 Tashkent earthquake ($M = 5.3$) and (B) an aftershock at Tashkent, $M = 4$. Arrows denote the origin times of the shocks.

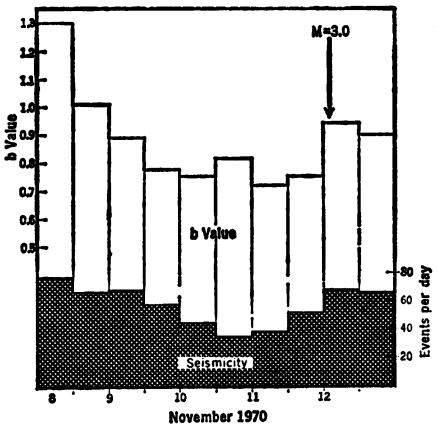

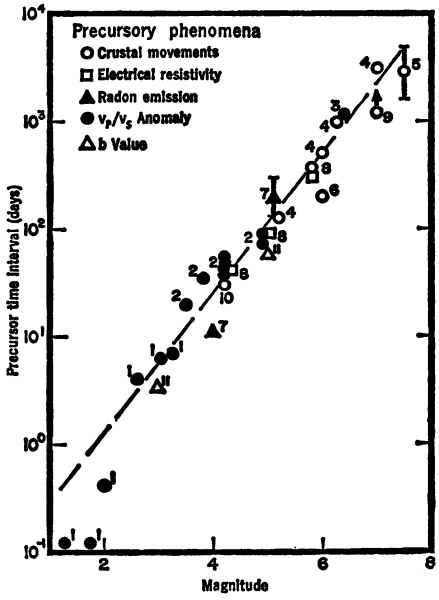

Fig. 7 (left). Observation of a drop in b value (top histogram) and seismicity rate (bottom histogram) for one of the larger aftershocks of the 1970 earthquake at Fairbanks, Alaska. Data from (*19*).

Fig. 8 (right). Duration time of various precursory phenomena as a function of earthquake magnitude. Earthquake location and data sources are as follows: point 1, Blue Mountain Lake, New York (*2*); point 2, Garm, U.S.S.R. (*1*); point 3, San Fernando, California (*3*); point 4, Kitamino, Kita-Izu, and Omi, Japan (*24*); point 5, Niigata, Japan (*13*); point 6, Odaigahara, Japan (*15*); point 7, Tashkent, U.S.S.R. (*17*); point 8, Garm, U.S.S.R. (*10*); point 9, Alma Ata, U.S.S.R. (*25*); point 10, Danville, California (*16*); and point 11, Fairbanks, Alaska (*19*).

value of 1.61 were measured in the hypocentral region of the Tashkent earthquake, as compared with more normal values for v_p of 6.2 and for v_p/v_s of 1.78 measured elsewhere in the Tashkent region (*18*). This finding certainly provides strong additional evidence for dilatancy.

Laboratory data indicate that the b value should decrease with increasing effective differential stress (*12*). Therefore we should expect that the b value would decrease during dilatancy hardening in stage II and increase again at the end of stage III. Exactly this behavior has been observed to precede several earthquakes in Alaska and California (*19*). A good example (Fig. 7) was obtained for an $M = 3$ aftershock of the 1970 Fairbanks earthquake. The aftershock was the largest event to have occurred in several months, and the large number of aftershocks made it possible to obtain accurate b value determinations for the earthquakes which occurred during each 24-hour period. The results showed a pronounced drop in the b value beginning 3 to 4 days prior to the earthquake. Moreover, the seismicity dropped to a level nearly half its normal value, showing the dilatancy-hardening effect (Fig. 7).

In nearly all the cases outlined above, only one type of the precursory phenomena was observed. The most direct evidence that these diverse precursory phenomena are due to the same cause is the fact that four different types of these phenomena were observed to precede an $M = 6$ earthquake in the Garm region in early 1969 (*20*).

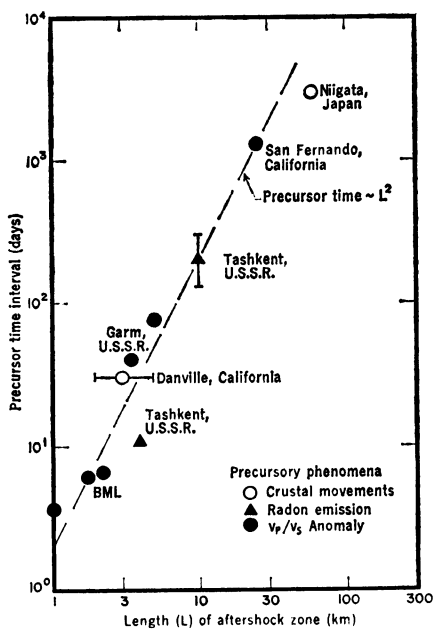

Fig. 9. Precursor time interval as a function of the length of the aftershock zone for a variety of earthquakes and types of physical observations. Note that a precursor time proportional to L^2 supports the model of the diffusion of fluids in the dilated zone. Data sources are the same as those in Fig. 8.

Fourteen months before that earthquake a marked reduction of local seismicity began to occur almost simultaneously with an anomalous crustal uplift. A v_p/v_s anomaly and an electrical resistivity anomaly were also observed for the same event. In this case, the beginning of the anomaly was accompanied by an increase of resistivity, followed by a decrease in resistivity which continued until the earthquake. This may indicate that, in the early stages, production of dry cracks (which would increase resistivity) at first outpaced their filling with pore fluids.

Time Duration of Precursory Phenomena

The logarithm of the duration (τ) of precursory effects of five different types are plotted as a function of M in Fig. 8 for more than 30 earthquakes. The various points fall close to a straight line. Thus, an estimate of the time duration of precursory events during stages II or III of the earthquake cycle could make possible a prediction of the magnitude of the approaching earthquake. The close agreement of precursor times for the same magnitude strongly suggests that a common physical mechanism causes each of the observed anomalies.

Additional support for a causal mechanism that involves the diffusion of cracks and fluids near the source region is obtained by plotting τ as a function of a characteristic length L. In Fig. 9 L is the longest dimension of the aftershock zone of the earthquakes. Although L is undoubtedly smaller than the size of the dilated region, the two dimensions are likely to be proportional to one another over a large range of magnitudes. The data in Fig. 9 are a good fit to $\tau = L^2/c$, a dependence expected from the diffusion equation describing flow in a porous medium

$$\frac{\partial P}{\partial t} = c\nabla^2 P \qquad (1)$$

where P is the fluid pressure and t is the time. The hydraulic diffusivity, a constant, is $c = k/\eta\phi\beta$, where k is the permeability of the rock; η is the viscosity of the pore fluid, here taken to be water; ϕ is the porosity; and β is the compressibility of water. The rock matrix is assumed to be incompressible. Taking $c = 5.8 \times 10^4$ square centimeters per second from Fig. 9, $\beta = 3.2 \times 10^{-5}$ per bar, $\phi = 10^{-3}$, and $\eta = 10^{-2}$ poise, we obtain $k = 2$ millidarcys (1 milli-

darcy = 10^{-11} square centimeter). This value is intermediate between the value 0.35×10^{-3} millidarcy for laboratory specimens of Westerly granite at a confining pressure of 100 bars (*21*) and the value 10^{3} millidarcys for fractured and jointed rocks (*22*). The computed permeability will, of course, be larger if the porosity is greater than 10^{-3}. Nevertheless, the computed value is not unreasonable for a dilated volume of rock that contains a major fault but which is neither completely fractured and jointed nor wholly unfractured. The surprisingly small scatter in Fig. 9 for data from various regions is probably related to the presence of cracks, which tend to increase the permeability to a value that is not strongly a function of lithology or of the permeability of the unfractured rocks.

Size of the Dilatant Volume

Clearly, much more work will need to be done to fully demonstrate the validity and degree of universality of precursory dilatancy. It is hoped that this article will point out the types of measurements that need to be made on a more thorough basis. One of the major questions to be resolved is the spatial extent of the dilatant region. The observations prior to the Niigata earthquake (*13*) indicate that dilatancy extended over a region of approximately two fault lengths in dimension. The v_P/v_S anomalies at Garm and San Fernando, however, were observed at seismographic stations considerably farther from the epicenter. At Garm, for example, most stations were concentrated in the distance range of 15 to 45 kilometers, and v_P/v_S anomalies were observed for earthquakes as small as $M = 4.5$, which would be associated with fault dimensions of only several kilometers (*1, 10*). Furthermore, only a few earthquakes close to the epicenter of the impending larger Garm events produce anomalously low v_P/v_S ratios, a result which suggests that the dilatant volume is localized.

This finding appears at first contradictory of the dilatancy hypothesis, but it can be shown that apparent low v_P/v_S ratios can be observed at stations entirely outside the dilatant region and that these low values are due to ray-focusing and refraction. Stations outside the dilatant zone will always register a smaller drop in v_P/v_S than that which occurs within the anomalous zone itself. Furthermore, the sampling will be more sporadic outside the dilatant zone, since only earthquake sources at particular locations within or near the dilatant zone show low v_P/v_S ratios. These features become apparent if one compares the Garm results with the BML observations, where all the seismic stations were within 6 kilometers of the epicenter. At BML, all events within the seismic network produced low v_P/v_S ratios, and the magnitudes of the drop in v_P/v_S (and in v_P itself from quarry blasts) were about twice those observed at Garm or San Fernando. The region enclosing all earthquakes that produced anomalous v_P/v_S ratios at Garm appears to be considerably smaller than the total dilatant zone, as indicated by electrical resistivity measurements. For an earthquake of magnitude 4.5, the width of the earthquake region was 5 kilometers (*10*), whereas the width of the dilatant zone was greater than 15 kilometers (*23*). It therefore seems likely that the earthquakes that produced anomalous v_P/v_S ratios at Garm were localized within the dilatant region in such a way as to produce optimal focusing. Thus, in general, the dimension of the dilatant volume appears to be several fault lengths. Hence, close seismic observations and detailed information on the geometry of source, receiver, and dilatant region are very important in the detection of anomalies in v_P/v_S.

Conclusions

The dilatancy instability that we have described appears to account for the entire class of long-range earthquake precursors yet observed. It thus seems commonly applicable in at least some types of tectonic regimes, for example, those involving a significant component of thrust faulting and those where complications or conditions exist such as to allow the stress to rise to high values. It is possible that stresses along simple strike-slip faults such as in central California will not rise high enough to initiate dilatancy; however, the Danville earthquake (*16*), which was preceded by anomalous tilts, had a strike-slip mechanism.

We suggest that the dilatancy mechanism is an instability from which there is apparently no return to stage I without the occurrence of an earthquake. In this sense dilatancy and fluid flow cause or trigger the earthquake. This process seems to be deterministic rather than probabilistic, like many aspects of weather prediction. This encourages us to believe that the number of "false alarms" in predicting earthquakes may well be small. This should especially be so if a variety of physical measurements are used as predictors. Furthermore, this process has the unique property that there is a longer warning time for a greater disaster. The use of v_P/v_S measurements alone yields the approximate time (to within about 10 percent of the total precursor time), the location, and the magnitude of the earthquake. It thus appears that this method holds great promise for providing a practical means of predicting earthquakes.

References and Notes

1. I. L. Nersesov, A. N. Semonova, I. G. Simbireva, in *Physical Basis of Foreshocks* (Nauka, Moscow, 1969); A. N. Semenov, *Izv. Earth Phys.* (English transl.), No. 4, 72 (1969).
2. Y. P. Aggarwal, L. R. Sykes, J. Armbruster, M. L. Sbar, *Nature* **241**, 101 (1973).
3. J. H. Whitcomb and J. D. Garmany, in preparation.
4. A. Nur, *Bull. Seismol. Soc. Amer.* **62**, 1217 (1972).
5. Relevant laboratory studies of dilatancy and its effects include the following: W. F. Brace, B. W. Paulding, Jr., C. H. Scholz, *J. Geophys. Res.* **71**, 3939 (1966); C. H. Scholz, *ibid.* **73**, 1417 (1968); W. F. Brace, *ibid.* **70**, 391 (1965); ——— and A. S. Orange, *ibid.* **73**, 1433 (1968); *Science* **153**, 1525 (1966); W. F. Brace and R. J. Martin III, *Int. J. Rock Mech. Min. Sci.* **5**, 415 (1968).
6. A. Nur and G. Simmons, *Earth Planet. Sci. Lett.* **7**, 183 (1969).
7. F. C. Frank, *Rev. Geophys.* **3**, 485 (1965).
8. J. H. Healy, W. W. Rubey, D. T. Griggs, C. B. Raleigh, *Science* **161**, 1301 (1968); J. H. Healy, W. H. K. Lee, L. C. Pakiser, C. B. Raleigh, M. D. Wood, *Tectonophysics* **14**, 319 (1972); L. R. Sykes, P. J. Fletcher, J. Armbruster, J. F. Davis, *Eos Trans. Amer. Geophys. Union* **53**, 524 (1972); *Earthquakes Related to Reservoir Filling* (National Academy of Sciences, Washington, D.C., 1972).
9. J. Byerlee, *J. Geophys. Res.* **72**, 3639 (1967).
10. M. A. Sadovsky, I. L. Nersesov, S. K. Nigmatullaev, L. A. Latynina, A. A. Lukk, A. N. Semenov, I. G. Simbireva, V. I. Ulomov, *Tectonophysics* **14**, 295 (1972); O. M. Barsukov, *ibid.*, p. 273.
11. C. H. Scholz, *ibid.*, p. 201; ———, P. Molnar, T. Johnson, *J. Geophys. Res.* **77**, 6392 (1972).
12. C. H. Scholz, *Bull. Seismol. Soc. Amer.* **58**, 399 (1968); M. Wyss, *Geophys. J. Roy. Astron. Soc.* **31**, 341 (1973).
13. Sea level data were those corrected for oceanographic and meteorological conditions by S. Yamaguti [*Bull. Earthquake Res. Inst. Tokyo Univ.* **46**, 1269 (1968)]. Leveling data are from V. Tsubokawa, T. Dambara, A. Okada [in *General Report on the Niigata Earthquake*, H. Kawasumi, Ed. (Tokyo Electrical Engineering College Press, Tokyo, 1968), p. 129].
14. T. Yukutake, in *General Report on the Niigata Earthquake*, H. Kawasumi, Ed. (Tokyo Electrical Engineering College Press, Tokyo, 1968), p. 141.
15. E. Nishimura, *Jishin* **14**, 260 (1961); ——— and Y. Tanaka, in *Geophysical Papers Dedicated to Kenzo Sassa* (Kyoto Univ. Press, Kyoto, 1963), p. 365.
16. M. D. Wood and R. V. Allen, *Bull. Seismol. Soc. Amer.* **61**, 1801 (1971); W. H. K. Lee, M. S. Eaton, E. E. Brabb, *ibid.*, p. 1771.
17. V. I. Ulomov and B. Z. Mavashev, in *The Tashkent Earthquake of 26 April 1966* (Akademiia Nauk Uzbekskoi, S.S.R., FAN, Tashkent, 1971), p. 188.
18. I. V. Pomerantseva and L. S. Shumilina, in *Physical Basis of Seeking Methods of Predicting Earthquakes*, M. A. Sadovsky, Ed. (O.I.U. Schmidt Instituta Fizicheskaya Zemli, Akade-

mia Nauk, U.S.S.R., Moscow, 1970), p. 83.
19. J. D. Van Wormer and L. Gedney, personal communication; J. Bufe, *Earthquake Notes* **42**, 1 (1971).
20. I. L. Nersesov, personal communication; ———, A. A. Lukk, V. S. Ponomarev, T. G. Rautian, B. G. Rulev, A. N. Semenov, I. G. Simbireva, in *Earthquake Precursors*, M. A. Sadovsky, Ed. (VINITI, Moscow, 1973), p. 72.
21. W. F. Brace, J. B. Walsh, W. T. Frangos, *J. Geophys. Res.* **73**, 2225 (1968).
22. A. Nur and J. R. Booker, *Science* **175**, 885 (1972).
23. O. M. Barsukov, P. D. Krasnyuk, N. A. Listov, O. N. Sorokin, in *Earthquake Precursors*, M. A. Sadovsky, Ed. (VINITI, Moscow, 1973), p. 207.
24. T. Rikitake, *Tectonophysics* **8**, 81 (1969).
25. Yu. D. Boulanger, A. K. Pevnev, V. B. Enman, P. A. Atrushkevich, E. N. Antonenko, *ibid.* **14**, 183 (1972).
26. We gratefully acknowledge the long efforts made by many scientists to detect premonitory effects of earthquakes. Data from Japan and the U.S.S.R. were particularly valuable in our study. L.R.S. acknowledges the opportunity to become acquainted with earthquake prediction research in the U.S.S.R. in 1971 as a guest of the Soviet Academy of Sciences at the center for earthquake studies in Garm, Tadjik, S.S.R. We thank J. H. Whitcomb and J. D. Garmany for providing a copy of their paper prior to publication. We thank P. Richards and M. Talwani for critical comments on the manuscript. Supported by the National Science Foundation (grants GA 36357x and GA 37093x) and U.S. Geological Survey (grant GS3). Lamont-Doherty Geological Observatory contribution No. 1939.

Miniature Eye Movement

The pattern of saccades made by man during maintained fixation may be a refined but useless motor habit.

Robert M. Steinman, Genevieve M. Haddad,
Alexander A. Skavenski, Diane Wyman

When a human being is asked to fixate, he rotates his eye causing the image of the fixation target to fall within his foveal bouquet—the part of his retina where he sees details best. If he is then asked to maintain fixation on the target, his eye makes a consistent but idiosyncratic pattern of slow and fast miniature eye movements. This maintained fixation pattern has traditionally been considered to be "involuntary," "spontaneous," or "reflexive," largely because these eye movements are extremely small (much smaller than ordinary voluntary motor acts), and also because the individual is not ordinarily aware of intending to make or of actually making any of these small eye movements (*1*). We believe that the traditional view is not entirely correct.

A typical maintained fixation pattern of a human being is shown in Fig. 1. This pattern is composed of three kinds of movements: saccades, drifts, and physiological nystagmus. Saccades are small, very fast changes in eye position. They occur one to three times each second, shifting the line of sight abruptly by a small amount. Their average size is about 6 minutes of arc (the same size as the head of a thumbtack 2.5 meters away from the eye). The eye slowly drifts back and forth in the intervals between saccades. These saccades and drifts are superimposed upon a high frequency tremor called physiological nystagmus (*2–4*). All subjects make these three kinds of miniature eye movements but the size and most frequent direction of saccades vary considerably from subject to subject.

Although the eye is continually moving, it does not wander very far from its mean position during maintained fixation (standard deviations are only about 2 to 5 minutes of arc on both horizontal and vertical meridians). This permits the retinal image of the target to remain within the foveal bouquet where detail vision is best and relatively uniform (the foveal bouquet has a diameter of about 20 minutes of arc) (*5*).

Dr. Steinman is professor of psychology at the University of Maryland, College Park 20742. Dr. Haddad is a research associate in the Department of Psychology at the University of Maryland. Dr. Skavenski is an assistant professor of psychology at Northeastern University, Boston, Massachusetts 02115. Dr. Wyman is a U.S. Public Health Service postdoctoral fellow in the Department of Ophthalmology, George Washington University Medical Center, Washington, D.C. 20037.

Origin of Modern Interest in Miniature Eye Movements

Modern interest in the fine details of the maintained fixation pattern was provoked by dynamic theories of visual acuity first proposed by Weymouth *et al.* (*6*) about 50 years ago and developed by Marshall and Talbot (*7*) and Jones and Higgins (*8*) in the 1940's. It is assumed in such theories that physiological nystagmus and reciprocal overlap in the visual pathways sharpen a target image blurred by optical defects of the normal human eye. The tremor causes the target image to sweep rapidly back and forth across a number of receptors. The cortex averages messages from the maximally stimulated population of these receptors. This average restores edges given only as shifting gradients of illumination in the blurred retinal image. Quantitative details of this theory were based on findings that were accepted as accurate estimates of physiological nystagmus made by Alder and Fliegelman who measured tremor by photographing light reflected from a small mirror resting on the limbus of the fixating eye (*9*). These authors reported that physiological nystagmus had a frequency of 50 to 100 hertz and an average amplitude of slightly more than 2 minutes of arc (such characteristic frequencies and amplitudes are required if eye movements are to provide the proposed statistical sharpening mechanism). The Marshall-Talbot dynamic theory of visual acuity was extended by Osgood and Heyer (*10*) in whose hands it became a statistical theory of form perception, an alternative to the volume conductor brain model which had been proposed by Köhler and Wallach a few years earlier (*11*). At about the same time, Riggs and co-workers in this country and Ditchburn and co-workers in England (*12*) as well as Yarbus in Russia (*13*) devised techniques to measure miniature eye movements during